Temporal and spatial variability of the sea surface salinity in the Nordic Seas

Tore Furevik,[1,2] Mats Bentsen,[1] Helge Drange,[1] Johnny A. Johannessen,[1,2] and Alexander Korablev[3]

Received 27 August 2001; revised 8 March 2002; accepted 25 March 2002; published 2 November 2002.

[1] In this paper, the temporal and spatial variability of the sea surface salinity (SSS) in the Nordic Seas is investigated. The data include a Russian hydrographical database for the Nordic Seas and daily to weekly observations of salinity at Ocean Weather Station Mike (OWSM) (located at 66°N, 2°E in the Norwegian Sea). In addition, output from a medium-resolution version of the Miami Isopycnic Coordinate Ocean Model (MICOM), forced with daily National Center for Environmental Prediction/National Center for Atmospheric Research (NCEP/NCAR) reanalysis data, is used to complement the analysis of the temporal and spatial fields constructed from the observational data sets. The Nordic Seas show a strong seasonal variability in the vertical density stratification and the mixed layer (ML) depth, with a weak stratification and a several hundred meters deep ML during winter and a well-defined shallow ML confined to the upper few tens of meters during summer. The seasonal variability strongly influences the strength of the high-frequency variability and to what extent subsurface anomalies are isolated from the surface. High-frequency variability has been investigated in terms of standard deviation of daily SSS, calculated for the different months of the year. From observations at OWSM, typical winter values range from 0.03 to 0.04 psu and summer values range from 0.06 to 0.07 psu. Results from the model simulation show that highest variability is found in frontal areas and in areas with strong stratification and lowest variability in the less stratified areas in the central Norwegian Sea and south of Iceland. Investigation of the interannual variability over the last 50 years shows a marked freshening of the Atlantic Water in the Norwegian and Greenland Seas. Moreover, the strength of the southern sector of the Polar front, as defined by the 34.8–35.0 psu isohalines along the western boundary of the inflowing Atlantic Water, undergoes significant interannual variability with gradient stretching reaching up to 300 km. In comparison, the variability in the strength of the eastern front and northern sector of the Polar front, seemingly controlled by the shelf break off Norway and the ridge between the Norwegian and the Greenland Seas, typically undergoes stretching only between 60 and 80 km. The investigation also demonstrates that the low-frequency variability in the upper ocean density field in the Greenland Sea, a key factor for the deep water convection, is governed by the variability in the sea surface field. Since the early 1960s, there has been a negative trend in the salinity, probably contributing to the observed decrease in the deep water production in that period. *INDEX TERMS:* 4215 Oceanography: General: Climate and interannual variability (3309); 4223 Oceanography: General: Descriptive and regional oceanography; 4255 Oceanography: General: Numerical modeling; 4572 Oceanography: Physical: Upper ocean processes; *KEYWORDS:* Nordic Seas, surface salinity, convection, fronts, interannual variability

Citation: Furevik, T., M. Bentsen, H. Drange, J. A. Johannessen, and A. Korablev, Temporal and spatial variability of the sea surface salinity in the Nordic Seas, *J. Geophys. Res.*, *107*(C12), 8009, doi:10.1029/2001JC001118, 2002.

1. Introduction

[2] The Nordic Seas [*Hurdle*, 1986] is the common name for the Greenland, Iceland, Norwegian, and Barents Seas (Figure 1). The region is bounded by the Arctic Ocean to the north, the deep North Atlantic Ocean to the southwest, and the shallow North Sea, Skagerrak Sea, and Baltic Sea to the southeast. The exchange of water masses across these boundaries, notably via the surface circulation pattern as well as the overflow of deep water, has a profound influence on the thermohaline conditions in the Nordic Seas, leading to a horizontal and vertical density structure unlike any other ocean region in the World.

[3] The salinity distribution in the Nordic Seas (Figure 1) is governed by the Norwegian Atlantic Current (NWAC), a

[1]Nansen Environmental and Remote Sensing Center, Bergen, Norway.
[2]Geophysical Institute, University of Bergen, Bergen, Norway.
[3]Arctic and Antarctic Research Institute, St. Petersburg, Russia.

0148-0227/02/2001JC001118$09.00

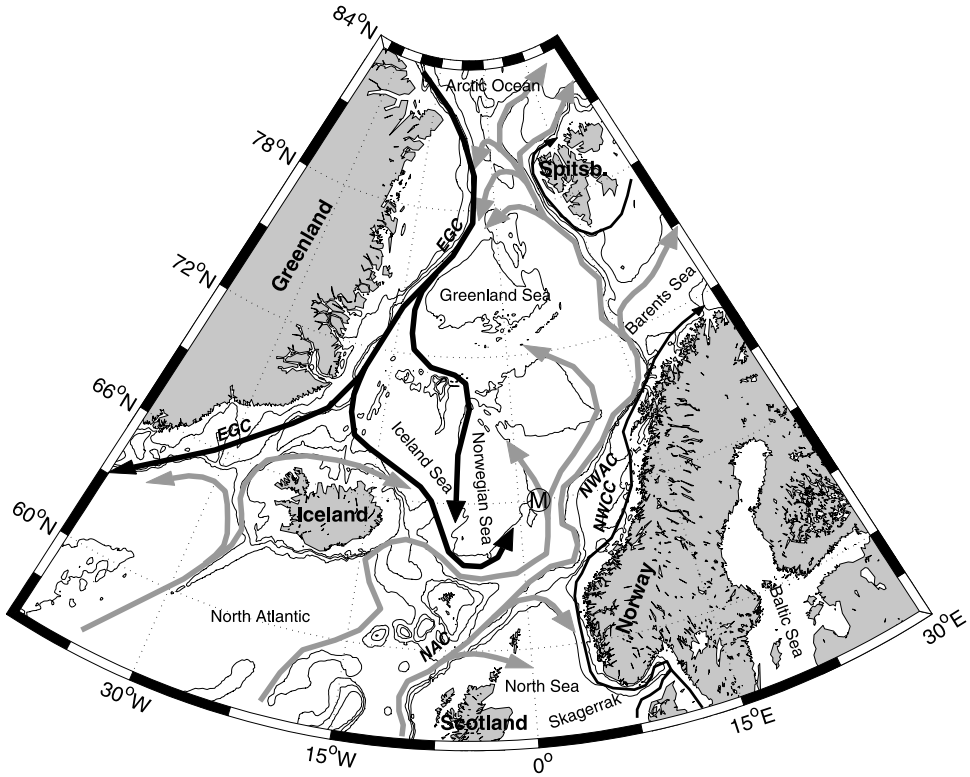

Figure 1. Map of the Nordic Seas. Isobaths are drawn at 250, 500, 1000, and 3000 m depths. Thick black arrows illustrate the flow of Polar Water, thin black arrows the flow of Coastal Water, and gray arrows the flow of Atlantic Water (see, for instance, the works of *Johannessen* [1986], *Hansen and Østerhus* [2000], and *Orvik et al.* [2001]). The M marks the position of the OWSM. The nomenclatures are defined in the text.

northward extension of the North Atlantic Current (NAC), and the East Greenland Currents (EGC) in addition to the local precipitation, runoff and evaporation fluxes. The former can typically be grouped according to the saline (i.e., >35 psu) inflow of Atlantic Water, and the cold and relatively fresh (i.e., <34 psu) outflow from the Arctic Ocean. Moreover, the fresh (i.e., 32–34 psu) water exiting by the Norwegian Coastal Current (NWCC) from the Baltic, Skagerrak and North Seas contributes to the salinity distribution along the eastern and north eastern sector of the Nordic Seas. As such the typical sea surface salinity (SSS) values in the Nordic Seas range from around 33 to 35.3 psu, approaching 32 psu near the coastal shelf regions as a result of sea ice melting and enhanced river runoff during summer.

[4] Climatological data analyzed by *Blindheim et al.* [2000] show that the zonal migration and position of the Polar front along 65°45′N undergoes significant seasonal to interannual variations. A maximum zonal position change of about 330 km was encountered between 1968 and 1993. They moreover showed that the dominant interannual variations are predominantly linked to the wind system, in their analysis represented by the North Atlantic Oscillation (NAO) winter index [*Hurrell*, 1995].

[5] The most persistent and extreme variation in the thermohaline conditions of the North Atlantic–Nordic Seas ever recorded, was a widespread freshening of the upper 500–800 m layer which occurred in the period from 1968 to 1982 [*Dickson et al.*, 1988]. First identified north of Iceland in the late 1960s, this anomaly is believed to cycle around the Atlantic subpolar gyre for more than a decade, finally returning to the Greenland Sea in the early 1980s. The largest salinity anomaly of ~0.5 psu was encountered in the Labrador Current, with weaker anomalies of ~0.1 psu found in the middle and eastern North Atlantic.

[6] The main objective for this study has been to give a comprehensive analysis of the SSS and its variability in the Nordic Seas. The paper is organized as follows: In section 2 the data sources, including both observational data and simulated fields, are described. The annual mean fields of salinity and temperatures are shown in section 3, and in section 4 the temporal and spatial SSS variability in the Nordic Seas are analyzed. In section 5 we investigate the vertical correlation of the salinity anomalies, and in particular the effects of SSS anomalies on the density anomalies and the deep water convection in the Greenland Sea. The paper is concluded in section 6.

2. Data Description

[7] Despite the fact that the Nordic Seas is among the longest and most well-sampled area in the World (going back to the pioneering work of *Helland-Hansen and Nansen* [1909]), the observational data cover is too coarse to give a good picture of the high-frequency variability in time (days to weeks) and space (10–100 km) of the upper ocean salinity. A Russian data set [*Johannessen et al.*, 2000], which to our knowledge offers the best data source, can be used to compile rather detailed maps of monthly climatol-

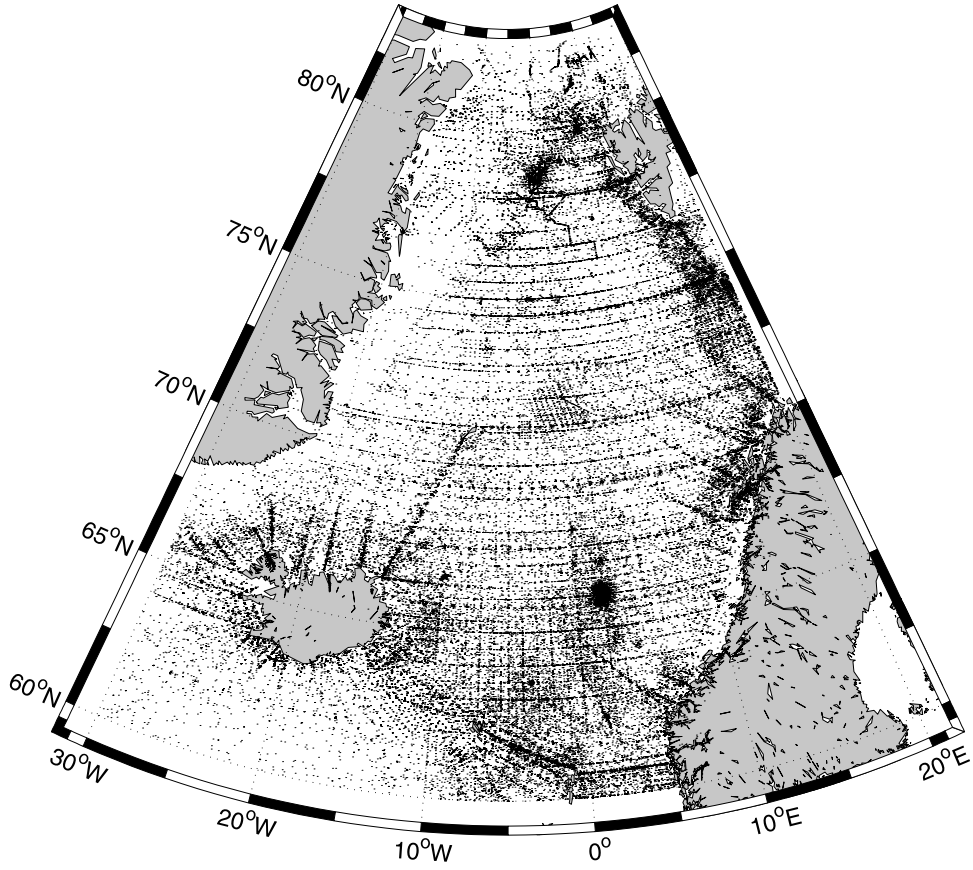

Figure 2. The spatial distribution of all hydrographical stations contained in the hydrographical database of the Nordic Seas. The total number of stations is 127,143.

ogy and interannual to decadal variability in the salinity in the Nordic Seas, but lack sufficient resolution in time. On the other hand, the hydrographical data set from the Ocean Weather Station Mike (OWSM) extends back to 1948, and provides time series with daily to weekly resolution of temperature and salinity [*Gammelsrød et al.*, 1992].

[8] In order to complement the observational data, output fields from a medium-resolution version of the Miami Isopycnic Coordinate Ocean Model (MICOM) has also been used to derive information on the temporal and spatial fields of SSS in the Nordic Seas. The model experiment was primarily designed to simulate the major modes of the natural variability of the ocean climate system, in particular the thermohaline circulation in the North Atlantic and the Nordic Seas. Hence, it allows investigation of the importance of the temporal and spatial variability of the SSS for the convective overturning and the deep water formation at high latitudes.

2.1. Observations

[9] The main source for the observational data has been an oceanographic database of the Norwegian and Greenland Seas compiled at the Arctic and Antarctic Research Institute, Department of Ocean/Atmosphere Interaction in St. Petersburg, Russia. The data set is mainly based on data from regular Russian cruises prior to the 1990s, and later on supplemented with data from the International Council for Exploration of the Sea (ICES) under the framework of the INTAS 97-1277 project [*Johannessen et al.*, 2000]. In total more than 127,000 hydrographical stations are included in this database. In addition more recent data from the OWSM, provided by the Geophysical Institute, University of Bergen, is included in the study.

[10] From the spatial distribution of the oceanographic database (Figure 2) it follows that the majority of the stations are from the eastern part of the Nordic Seas, where several standard hydrographic sections and the position of the OWSM (cluster at 66°N, 2°E) can be identified. Several standard sections in the Icelandic waters and in the Faroe Shetland Channel are also visible. In comparison, the data coverage south of Iceland and along the usually ice covered East Greenland continental shelf is rather sparse.

[11] The majority of the data is collected during the period 1950–1995 (Figure 3a), with a maximum of 5435 stations for the year 1984 and 4527 during 1989. Only data from 1920 and onward (125,443 stations) has been included in this study. The distribution by month (Figure 3b) shows a maximum in June, when the number of hydrographical stations exceeds 25,000 (20% of the total), and a minimum in December, when only 5106 stations are present (4% of the total).

[12] The hydrographical database consists of measurements of temperature, salinity, potential density and oxygen interpolated to 30 standard Levitus depths (0, 10, 20, 30, 50, 75, 100, 125, 150, 200, 250, 300, 400, 500, 600, 700, 800, 900, 1000, 1100, 1200, 1300, 1400, 1500, 1750, 2000, 2200, 2500, 3000, and 3500 m). For the purpose of this study, all measurements have been gridded into $1^\circ \times 0.5^\circ$

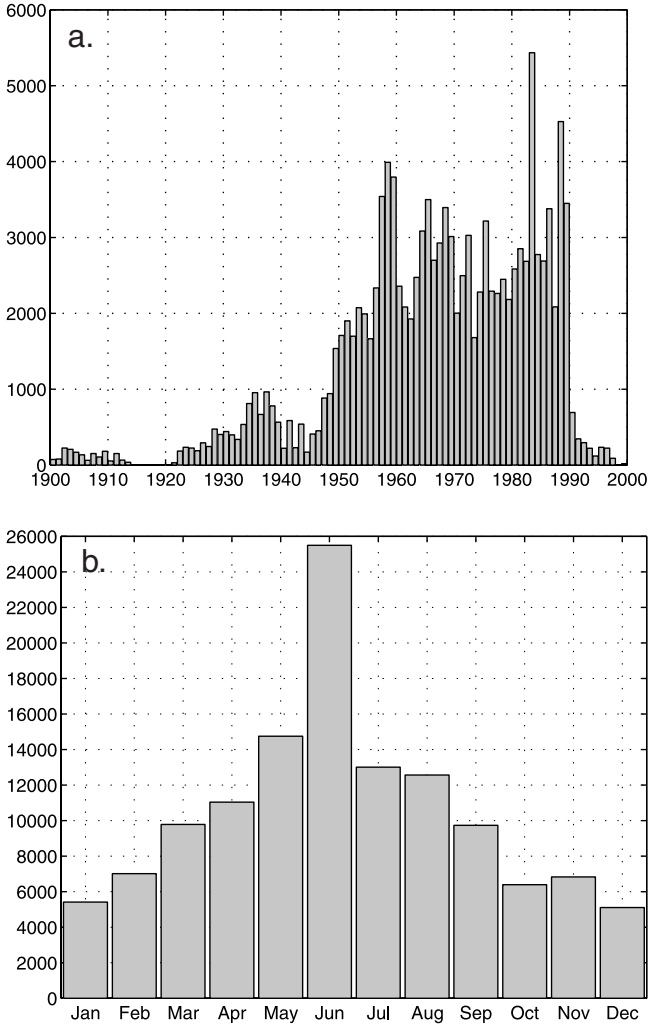

Figure 3. The total number of all hydrographical stations per year (a) and per month (b).

longitude–latitude boxes, ranging from approximately 55 × 55 km in the south to 15 × 55 km in the north. The climatological fields are then calculated by making monthly averages for each month of the year. Grid boxes containing no data have been filled by using a Gaussian 8 points weight function on the nearest neighbors. This may lead to artificial smoothing of the fields in areas with sparse data coverage, and in particular along the marginal ice zone and south of Iceland. For the central and eastern parts of the Nordic Seas, mainly in the Atlantic Water domain, the data coverage is generally good, and errors due to the interpolation will for this study be negligible. Anomalies are calculated by subtracting the local monthly climatology from the actual value.

2.2. Model Simulations

[13] The model was configured with a local horizontal orthogonal grid system with one pole over North America and the other pole over central Europe [*Bentsen et al.*, 1999]. By using a global grid with a focus area, no artificial boundary conditions are needed, in contrast to the case of a limited area model. Therefore, decadal and longer integrations are feasible without the classical problem of prescribing essential unknown temporal evolving boundary conditions. For the simulations described here, the horizontal grid resolution varies between 40 and 270 km, with 40–50 km resolution in the North Atlantic–Nordic Seas region, and the most degraded resolution in the South Pacific.

[14] The model has 26 layers in the vertical, of which the uppermost mixed layer (ML) has a temporal and spatial varying density. The specified potential densities of the subsurface layers were chosen to ensure proper representation of the major water masses in the North Atlantic/Nordic Seas region. The densities of the isopycnic layers (in σ_0 units) are 24.12, 24.70, 25.28, 25.77, 26.18, 26.52, 26.80, 27.03, 27.22, 27.38, 27.52, 27.63, 27.71, 27.77, 27.82, 27.86, 27.90, 27.94, 27.98, 28.01, 28.04, 28.07, 28.10, 28.85, and 29.10.

[15] The vertically homogeneous ML utilizes the *Gaspar* [1988] bulk parameterization for the dissipation of turbulent kinetic energy, and has temperature, salinity and layer thickness as the prognostic variables. In the isopycnic layers below the ML, temperature and layer thickness are the prognostic variables, whereas the salinity is diagnostically determined by means of the simplified equation of state of *Friedrich and Levitus* [1972]. The bathymetry is computed as the arithmetic mean value based on the ETOPO-5 database (Data Announcement 88-MGG-02, Digital relief of the Surface of the Earth, NOAA, National Geophysical Data Center, Boulder, CO, 1988).

[16] The thermodynamic module incorporates freezing and melting of sea ice and snow covered sea ice [*Drange and Simonsen*, 1996], and is based on the thermodynamics of *Semtner* [1976], *Parkinson and Washington* [1979], and *Fichefet and Gaspar* [1988]. The dynamic part of the sea ice module is based on the viscous plastic rheology of *Hibler* [1979], where sea ice is considered as a two-dimensional continuum. The dynamic ice module has been further modified by *Harder* [1996] to include description of sea ice roughness and the age of sea ice, and utilizing the advection scheme of *Smolarkiewicz* [1984].

[17] The continuity, momentum and tracer equations are discretized on an Arakawa C-grid stencil [*Arakawa and Lamb*, 1977]. The diffusive velocities (diffusivities divided by the size of the grid cell) for layer interface diffusion, momentum dissipation, and tracer dispersion are 0.015, 0.010, and 0.005 m s^{-1}, respectively, yielding actual diffusivities of about 10^3 m^2 s^{-1}. A flux corrected transport scheme [*Zalesak*, 1979; *Smolarkiewicz and Clark*, 1986] is used to advect the model layer thickness and the tracer quantities.

[18] The diapycnal mixing coefficient K_d (m^2 s^{-1}) is parameterized according to the *Gargett* [1984] expression $K_d = 3 \times 10^{-7}$ N^{-1}, where $N = \sqrt{\frac{g}{\rho}\frac{\partial \rho}{\partial z}}(s^{-1})$ is the Brunt-Väisälä frequency (here g (m s^{-2}) is the gravity acceleration, ρ (kg m^{-3}) is the density and z (m) is the depth). The numerical implementation of the diapycnal mixing follows the scheme of *McDougall and Dewar* [1998].

[19] For the simulations discussed here, the model was initialized by the January *Levitus and Boyer* [1994] and *Levitus et al.* [1994] climatological temperature and salinity fields, respectively, a 2 m thick sea ice cover based on the

climatological sea ice extent, and an ocean at rest. The model was then integrated for 30 years by applying the monthly mean National Center for Environmental Prediction/National Center for Atmospheric Research (NCEP/NCAR) atmospheric forcing fields, and thereafter forced with daily NCEP/NCAR reanalysis [*Kalnay et al.*, 1996] fields for the period 1948 to 1999. From the NCEP/NCAR reanalysis, wind stress, short wave, long wave, latent and sensible heat fluxes, precipitation, runoff, and sea level pressure fields are used. The momentum, heat and fresh water fluxes are modified when the modeled surface state (sea surface temperature (SST) and sea ice cover) differs from the NCEP/NCAR reanalysis surface state by applying the *Fairall et al.* [1996] bulk parameterization scheme [*Bentsen and Drange*, 2000].

[20] During the spin-up phase, the ML temperature and salinity were relaxed toward the monthly mean climatological values of *Levitus and Boyer* [1994] and *Levitus et al.* [1994], respectively, with a relaxation timescale of 30 days for a 50 m thick ML. The relaxation was reduced linearly with ML thicknesses exceeding 50 m, and it was set to zero in waters where sea ice is present in March (September) in the Arctic (Antarctic) to avoid relaxation toward temperature or salinity outliers in the poorly sampled polar waters. For the integration with daily fields, fresh water fluxes, diagnosed from the salinity relaxation with climatological fields, were added to the ML (M. Bentsen et al., Variability of the Atlantic meridional overturning circulation in an isopycnic coordinate OGCM, submitted to *Climate Dynamics*, 2002).

3. Mean Fields of Salinity and Temperature

[21] The distribution of water masses in the Nordic Seas as depicted by the model and observations, is characterized by three major fronts (Figures 4 and 5): The Iceland Gap front running from Iceland in a southeasterly direction, the Polar front having a meandering shape from east of Iceland toward Spitsbergen, and the Norwegian Coastal front controlled by the relatively straight shelf break along the coast of Norway. The three water masses related to the different current systems in the Nordic Seas are easily identified (compare with Figure 1). They are from west to east (1) the southward flow of fresh and cold Polar Water, having typical surface salinity below 34 psu and temperature below 3°C, (2) the northward flow of saline and warm Atlantic Water, with surface salinity and temperature above 35 psu and 5°C, respectively, and (3) off the Norwegian Coast, the fresh northward flow of Coastal Water, having surface salinity in the range 32–34 psu.

[22] The salinity minima are located in the east and west while the salinity maximum is found in the core of the northward flowing NWAC. In the meridional plane along the major (near northward) flow direction of the NWAC, on the other hand, the surface salinity decreases gently toward north. The Polar front enveloped by the 35.0–35.1 psu isohalines on average elongates in a northerly direction confined by the gradient region along the westward side of the NWAC.

[23] Averaged over 50–200 m depth (Figures 4c and 5c), annual mean salinities are generally higher than at the surface, and temperatures lower. The characteristic water mass structure is still evident, but with a much weaker Polar front, and with the Norwegian Coastal front displaced 100 km to the east. The salinity maximum at 50–200 m depth is to the east of the surface maximum, and below the western edge of the fresh Norwegian Coastal Water.

[24] Defined by the position of the 35 psu isohaline, the AW is confined to the upper 600 m (Figure 6). The salinity is seen to be a rather conservative property along the core of the AW flow, with values slowly decreasing from 35.3 psu in the inflowing area to slightly below 34.9 psu in the Greenland Sea. The depth of the salinity maximum slowly increases downstream at a rate of approximately 0.1 m km^{-1}.

[25] At the eastern side of the Nordic Seas, the temperature maximum is confined to the upper waters. In the recirculation area in the Fram Strait, the Atlantic Water flows beneath the fresher Polar Water, and here the depth of the temperature maximum is seen to increase toward the Greenland Sea.

[26] The model simulations capture only partly the main features of the flow field (Figures 4b, 4d, 5b, and 5d). Due to a weak negative drift in salinity over the last 50 years of integration (the NCEP/NCAR period 1948 to present), the annual mean salinity in the model is approximately 0.1 psu lower than what is found in the observations. Surface temperatures agree well with the observations except for in the central parts of the region, where they are too low. This could be linked to an overestimation of the mixing with the deeper, colder water masses in the model.

[27] As the northward flow of Atlantic Water has an eastward displacement compared to the observations (Figures 4a and 4b), the upper waters of the section along the AW flow becomes too fresh, and in particular the temperatures in the Norwegian Sea too low (Figure 6). The vertical mixing in the model seems to be too strong, making the subsurface saline core weaker than the observed one, and the front between the Atlantic and the Polar Waters in the Fram Strait region extending too deep (Figure 6b). A related problem is that the model fails to produce a realistic recirculation of Atlantic Water in the Fram Strait, and for this reason the salinity in the central Greenland Seas is too low.

4. Variability in the SSS

[28] In this section the variability in the SSS is discussed in the context of daily, seasonal, and interannual timescales. For variability with timescales less than one month, only the observational data from OWSM have sufficient temporal resolution to be used. Standard deviations calculated for 30 days blocks at this position are then compared to calculations based on the output from the model simulations. For seasonal to interannual timescales, the hydrographic database has been sufficient for the study, and has therefore been the only source of data for the given discussion.

4.1. Daily Variability

[29] The day-to-day variability has been investigated in terms of standard deviations of daily SSS and SST data calculated for 30 days blocks. Due to seasonal variations in the atmospheric forcing and in the thickness of the ML in the ocean, there is a clear seasonal pattern in the day-to-day variability of SSS and SST at OWSM (Figure 7), with

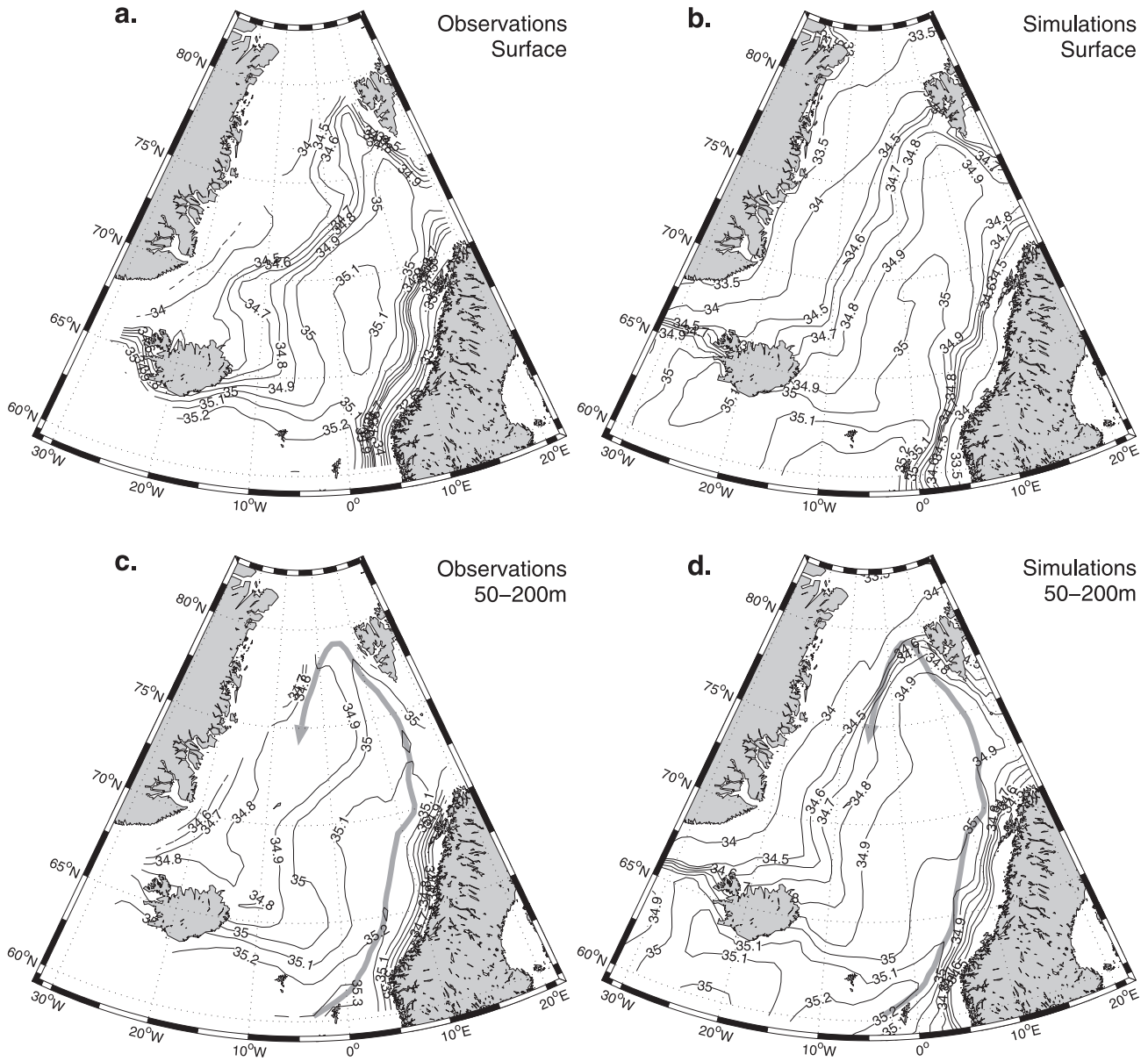

Figure 4. Annual mean salinity distribution at the surface (upper) and averaged over 50–200 m (lower) based on the observational data (left) and on the model simulations (right). Contours are drawn at 0.5 psu intervals below the 34.5 psu and at 0.1 psu intervals above this value. The observational data have been smoothed using a 3 × 3 points rectangular window. The gray arrow shows the deduced pathway of the Atlantic Water flow based on the observed 50–200 m salinity maximum.

lowest day-to-day variability found in March (0.03 psu), and highest in July (0.07 psu). While the seasonal signal for the SSS variability has a broad peak, with almost constant values during the summer months June to August, the corresponding signal for SST has a narrow primary peak in June, and a secondary peak in October.

[30] A fraction of the calculated standard deviations is evidently due to the seasonal variability in the time series, as a trend over a 30 day time period will give a contribution to the calculations made. However, subtraction of the seasonal cycle (calculated for all years) from the time series prior to the analysis, made negligible differences in the result for salinity, and only a 10–20% reduction in the calculated standard deviations for temperature (not shown).

[31] As for the OWSM data, the model simulations give that the maximum in sea surface variability is found during summer, and the minimum during winter. In Figure 8, the model realizations for March and September are shown. At the position of OWSM the model gives a temporal variability of 0.01 psu in March, and of 0.03 psu in September, compared to the 0.03 and 0.05 psu, respectively, based on the observations (Figure 7). A reason for the weaker variability in the simulated SSS is the relatively coarse resolution of the model compared to the Rossby deformation radius at these high latitudes, which makes the

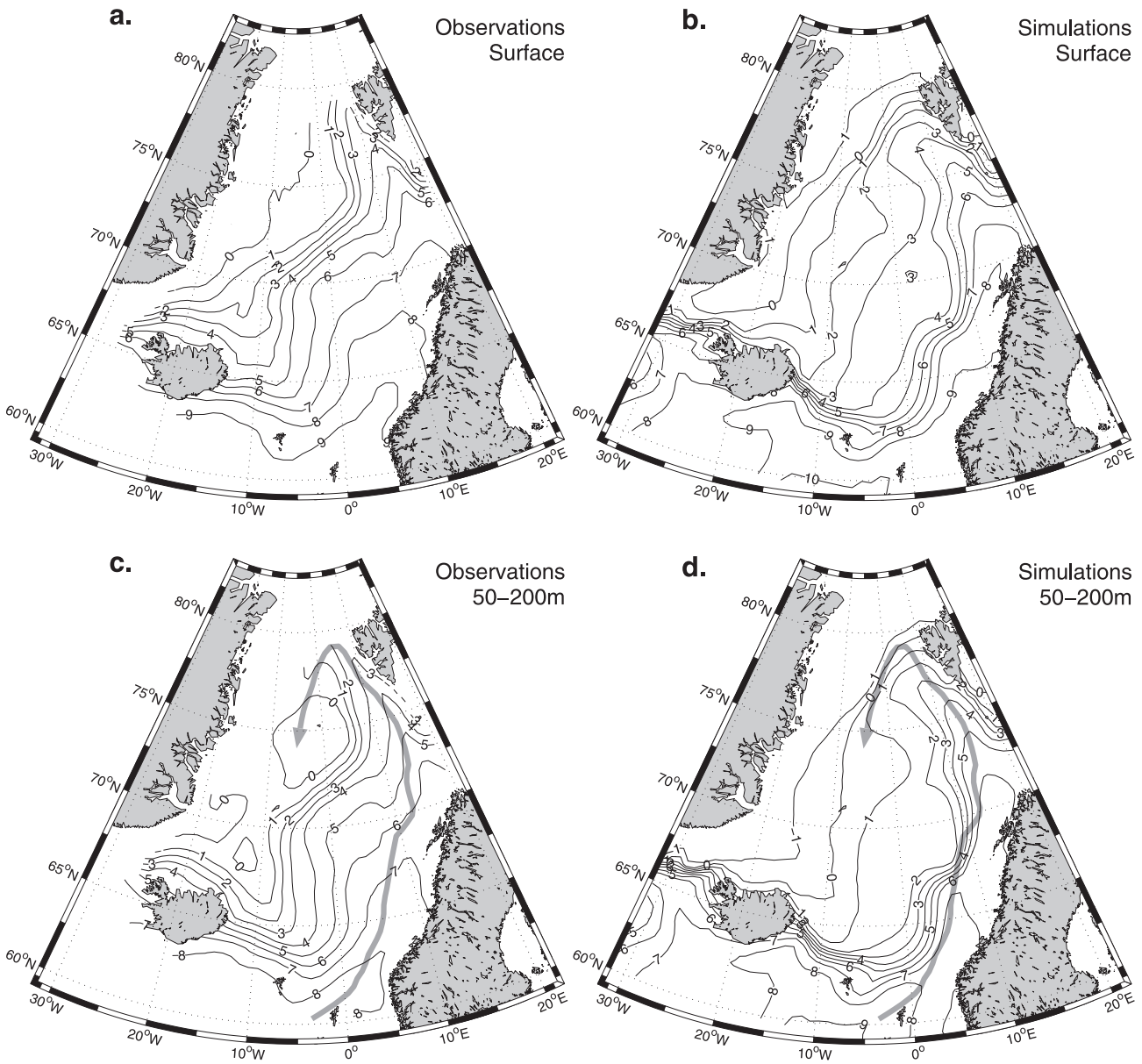

Figure 5. Annual mean temperature distribution at the surface (upper) and averaged over 50–200 m (lower) based on the observational data (left) and on the model simulations (right). Contours are drawn at 1°C intervals. The observational data have been smoothed using a 3 × 3 points rectangular window. The gray arrow shows the deduced pathway of the Atlantic Water flow based on the observed 50–200 m salinity maximum (Figure 4).

model unable to capture the mesoscale activities (eddies and meanders) in the area. As the spatial standard deviation in the area is near 0.03 psu in March and 0.08 psu in September, any mesoscale activities not resolved in the model, would give a significant contribution to the temporal SSS variability. It should also be noted that the eastward displacement of the Polar front in the model (see Figure 4), may have contributed to the lower variability found in the model.

[32] The similarity with the distribution of the standard deviation field and the simulated salinity field (Figures 4b and 4d), clearly indicates that a more stable water column due to lower surface salinity, leads to an enhanced variability in the surface properties. It follows that the highest variability is found in the western and northern part of the Nordic Seas, and along the coast of Norway. Lowest variability is found in the central parts of the region, and to the south of Iceland.

4.2. Seasonal Variability

[33] Based on the observations, the salinity field of the Nordic Seas shows largest seasonal signal in the surface waters, where the annual variability ranges from 0.2 psu in the central parts to more than 2 psu near the coasts of Norway and Greenland (Figure 9). However, the quality of the values in the usually ice covered waters near Greenland can be questioned as the observational data is here rather sparse (see Figure 2). The model generally underestimates

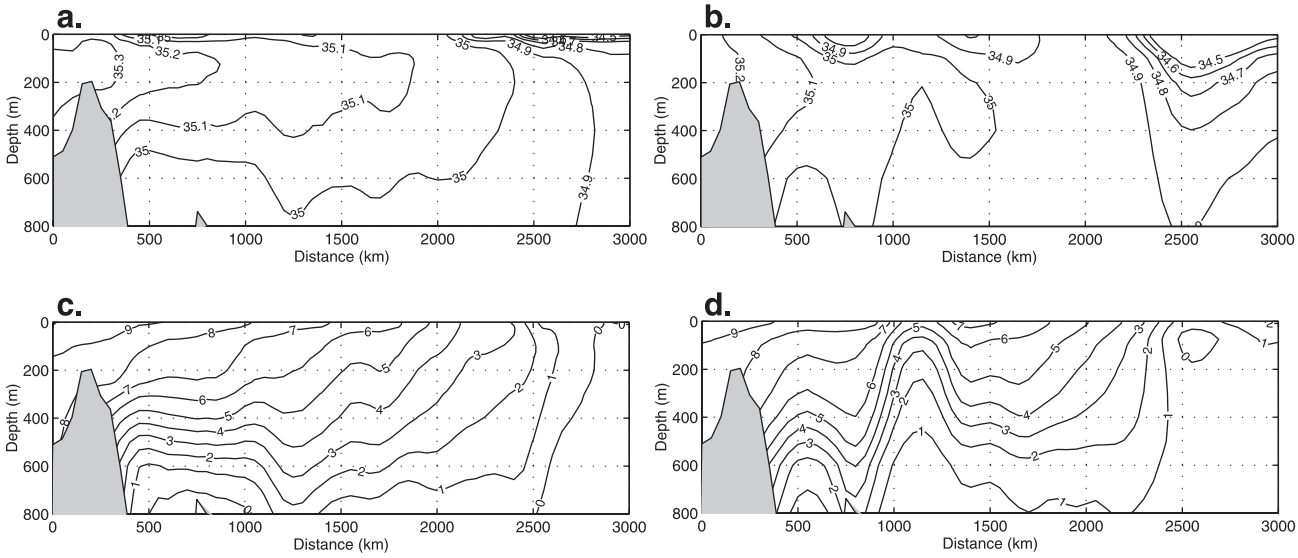

Figure 6. Annual mean salinity (upper) and temperature (lower) distribution in a section along the pathway of the Atlantic Water flow in the Nordic Seas (see Figures 4 and 5). Left are the observations, right the model data. The shaded bathymetry is the maximum depth in the corresponding $1^\circ \times 0.5^\circ$ grid cells based upon the ETOPO-5 database. The plots have been smoothed using a 3×3 points rectangular window.

the seasonal variability at the surface, in particular in the highly stratified coastal areas.

[34] Averaged over 50–200 m depth, the annual cycle ranges from 0.1 psu in the central parts of the region to 0.5 psu near the coasts. Here the model output is in better agreement with the observations. As a consequence, the model will typically underestimate the seasonal variability in the stratification near the surface.

[35] Maximum salinity at the surface is typically reached during late winter as a result of entrainment of saline subsurface waters, by brine release during freezing of sea ice, or near the coasts by a reduction of the runoff from the nearby land areas. Averaged over 50–200 m, the picture is more complex. At the western side of the Nordic Seas, the freezing and melting cycles of the sea ice dominate the salinity variability, with maximum values in January or February. At the eastern side, where the Atlantic and coastal waters are the major water masses, the annual cycle in the 50–200 m salinity is in opposite phase compared to the surface salinity. Here winter convection and mixing with fresher surface water tend to decrease the subsurface salinity maximum, and the salinity maximum is therefore found during August or September when the stratification is strong.

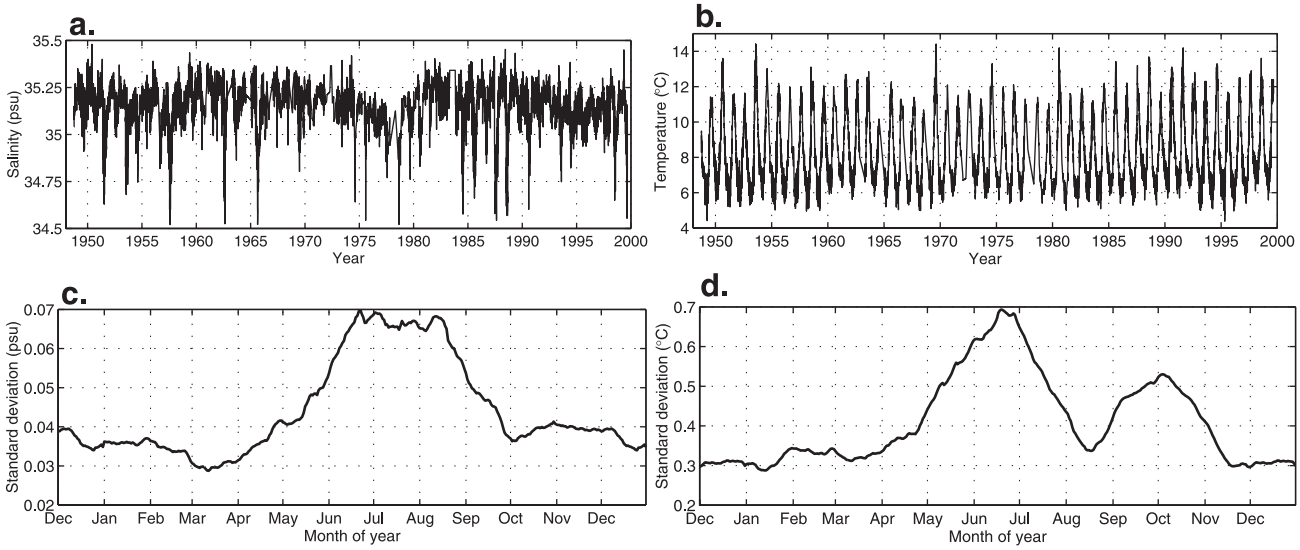

Figure 7. High-frequency variability of SSS (left) and SST (right) at OWSM. Upper row shows the raw data sets with daily to weekly resolution. Lower row shows the seasonal cycle of the standard deviation (day-to-day) calculated for sliding 30 day blocks.

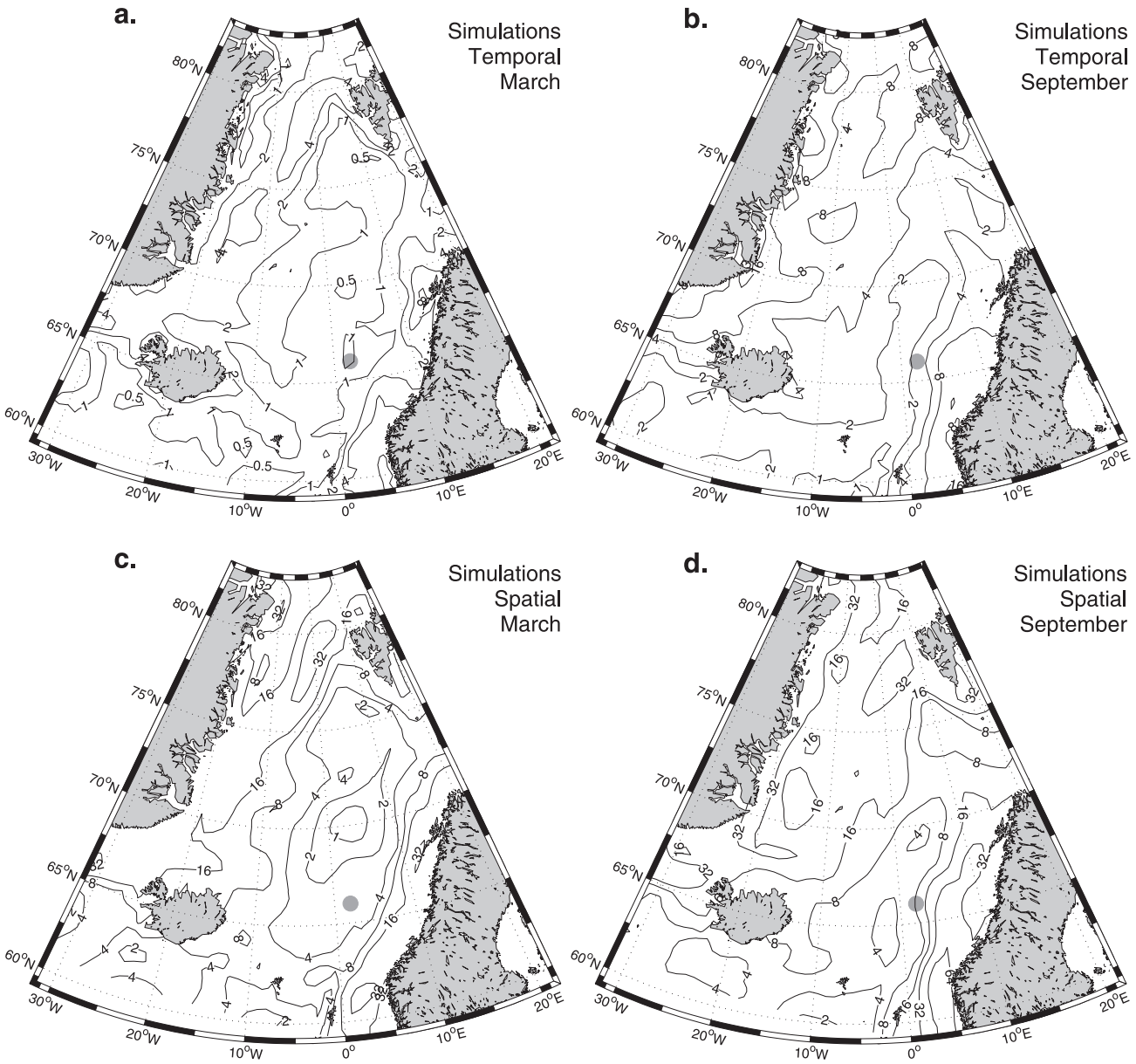

Figure 8. High-frequency variability of SSS in March (left) and September (right) based on the model simulations. Upper row shows the mean temporal standard deviations of the SSS calculated over all 30 day intervals with center in the particular month. Lower row shows the mean spatial standard deviation of the SSS calculated over boxes of 4 × 4 grid cells (approximately 200 × 200 km), thus expressing the strength of the fronts. Isolines (0.01 psu) are drawn on a base 2 log scale. The position of OWSM is marked with a gray dot.

[36] The out-of-phase seasonal cycles of the surface and the 50–200 m depth salinity in the Atlantic sector of the Nordic Seas, may be visualized by plotting the positions of selected isohalines (Figure 10). Even modest variability in salinity can give large spatial variability in the position of the 35.0 psu isohaline, frequently used to characterize the boundary between waters of Atlantic and Polar origin [e.g., *Blindheim et al.*, 2000]. In March, surface waters with salinity above 35.1 psu are found north to 71°N, compared to 63°N during summer. At 50–200 m depth (Figure 10b), the situation is different with salinity maximum occurring during summer, and minimum during winter. In addition, at 65°N in September, the 35.0 and 35.1 psu isolines are positioned 300 and 100 km, respectively, to the west compared to the March positions.

4.3. Interannual Variability

[37] In order to quantify the interannual variations in the SSS, 5 year averages have been calculated from the observed data set starting from 1950. Each 5 year period contained on the order of 10,000 hydrographical stations (see Figure 3a). Time averaging periods less than about 5 years showed too much noise in various locations. The trend of the last decades with a freshening of the Nordic Seas

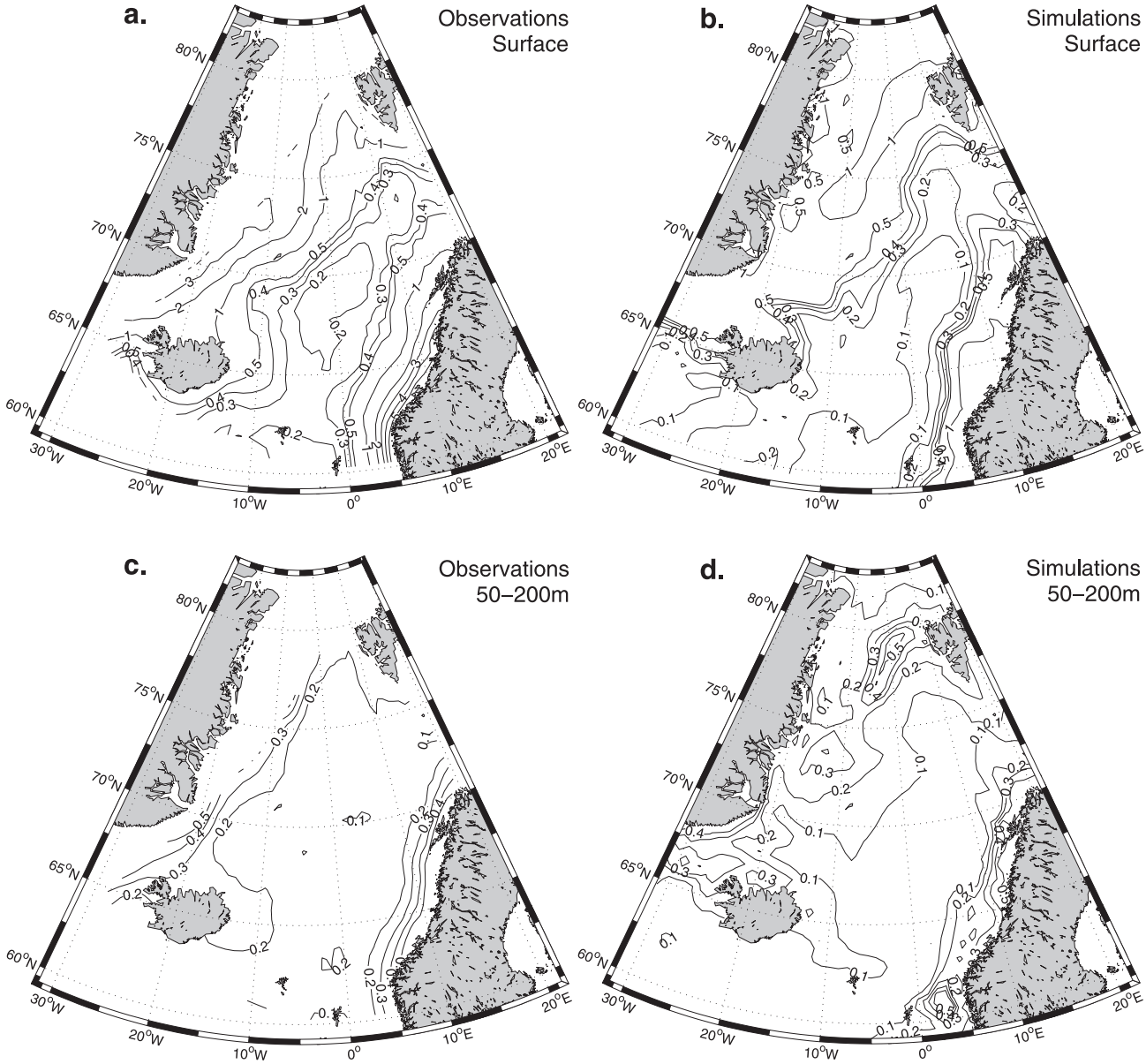

Figure 9. Seasonal variability in salinity based on observations (left) and simulations (right). The plots show the difference between maximum and minimum salinity (psu) based on the monthly climatologies. Upper row shows SSS, lower row the salinity averaged over 50–200 m depth.

[*Blindheim et al.*, 2000] and the minimum in the Atlantic Water salinity during the passage of the great salinity anomaly in the late 1970s [*Dickson et al.*, 1988] are found in the data set.

[38] Here we show the surface salinity at the two 5 year periods 1965–1969 and 1975–1979 (Figure 11). In the former period the surface salinity in the Atlantic Water part of the Nordic Seas was high, with the 35.0 and 35.1 isolines extending to 75°N and 72°N, respectively. During the latter period, the salinity shows a minimum with the 35.0 and 35.1 isolines positioned at 73°N and 63°N, respectively. The corresponding mean zonal displacement of the 35.0 isohaline between 65°N and 70°N on the western side of the salinity maximum is approximately 200 km. Note that the annual means of the SSS during the two climate extremes are very close to the March and September climatology (Figure 10).

[39] From the frontal locations and configurations of the 34.9–35.1 psu (see Figure 4a) isohalines for the Polar, the Norwegian shelf break and the Iceland Gap fronts, a qualitative picture can be drawn of the distribution of the Atlantic and Polar Waters, their influence on the heat exchange with the atmosphere, and possibly on impacts on the thermohaline convection of the Nordic Seas. For this, the interannual variations are calculated from averaging over 3 year periods, centered around each year. The front along the shelf break is clearly the most prominent, followed by the northern part of the Polar front (Figure 12). It appears that the steep shelf break off the coast of Norway strongly controls the position of the front, while the water masses defining the Polar front to the west display larger zonal migrations. In particular the position of the 35 psu isohaline

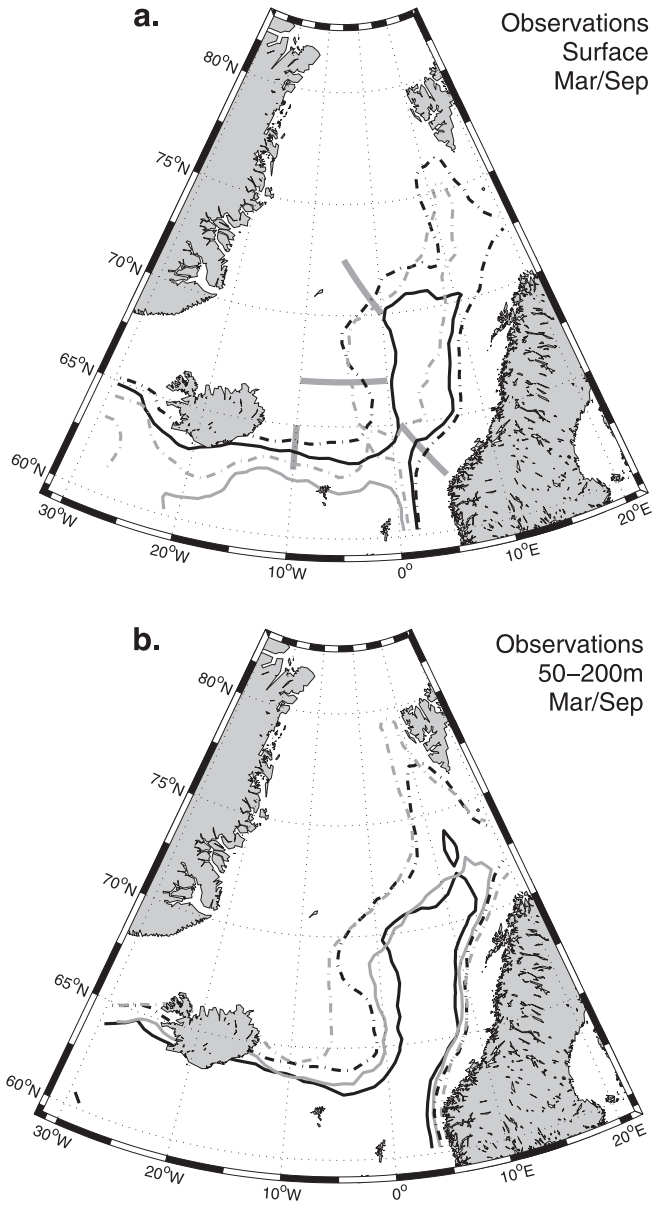

Figure 10. Observed monthly mean positions of the 35.1 (solid) and 35.0 (dashed) isohalines for March (black) and September (gray). Figure 10a shows the SSS, Figure 10b the salinity averaged over 50–200 m depth. Thick lines define the four sections shown in Figure 12.

(at 67°N) can undergo seasonal and interannual zonal displacements of up to 300 km while the corresponding displacements in the northern sector (at 71°N) rarely exceed 100 km. In comparison, the zonal displacement of the 35 psu isohaline at the Norwegian shelf break is typically less than 80 km. In 1964, waters above 35.0 psu were not present in the easternmost branch of the NWAC (see Figure 1). Moreover, for the southern part of the Polar front and the Iceland Gap front, long-periodic trends are also observed in frontal positions. These are qualitatively in agreement with the reported freshening and cooling of the central Nordic Seas since the 1960s [*Blindheim et al.*, 2000].

[40] A summary of the findings in this section, is given in Table 1. Here we have focused on the variability along the four sections defined in Figures 10a and 11a, and discuss both the standard deviation in the SSS and the displacement of the 35 psu isohaline.

[41] An empirical orthogonal function (EOF) analysis of the interannual variability of the SSS data was also performed. However, the combined effect induced by lack of dense and homogeneous data coverage (Figure 2) and relatively significant high-frequency variability in the western domain of the Nordic Seas (Figure 8) produced very complicated results. Consequently we were not able to draw any further conclusion about the interannual variability in

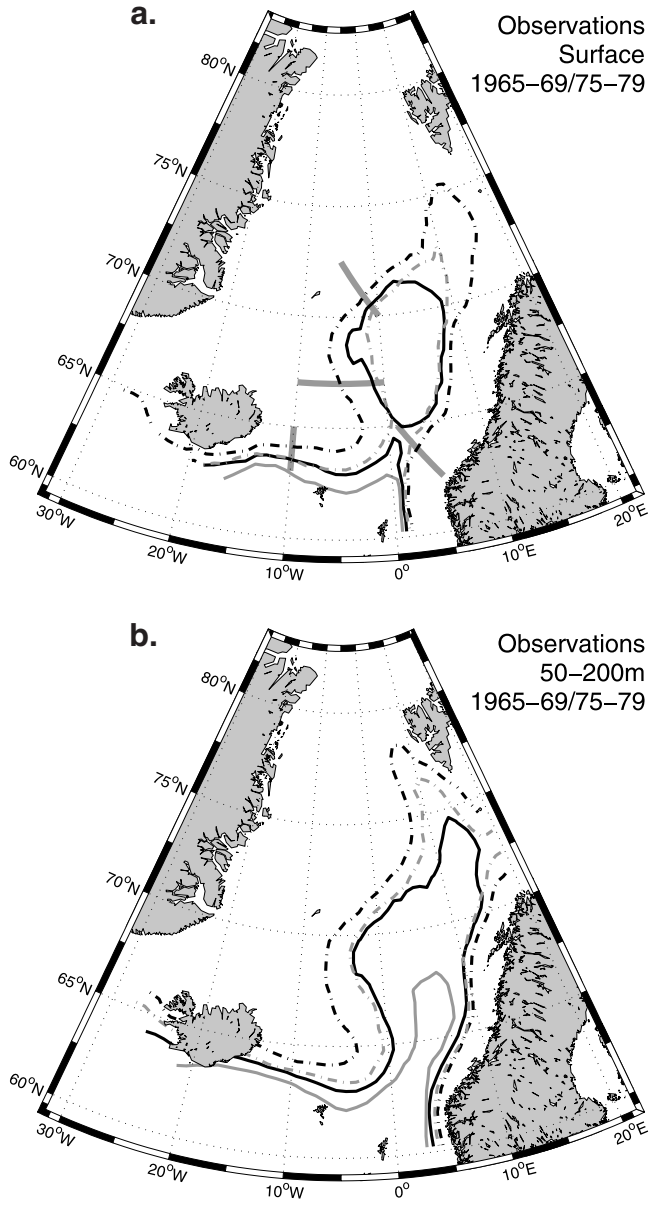

Figure 11. Observed annual mean positions of the 35.1 (solid) and 35.0 (dashed) isohalines for the periods 1965–1969 (black) and 1975–1979 (gray). Figure 11a shows the SSS, Figure 11b the salinity averaged over 50–200 m depth. Thick lines define the four sections shown in Figure 12.

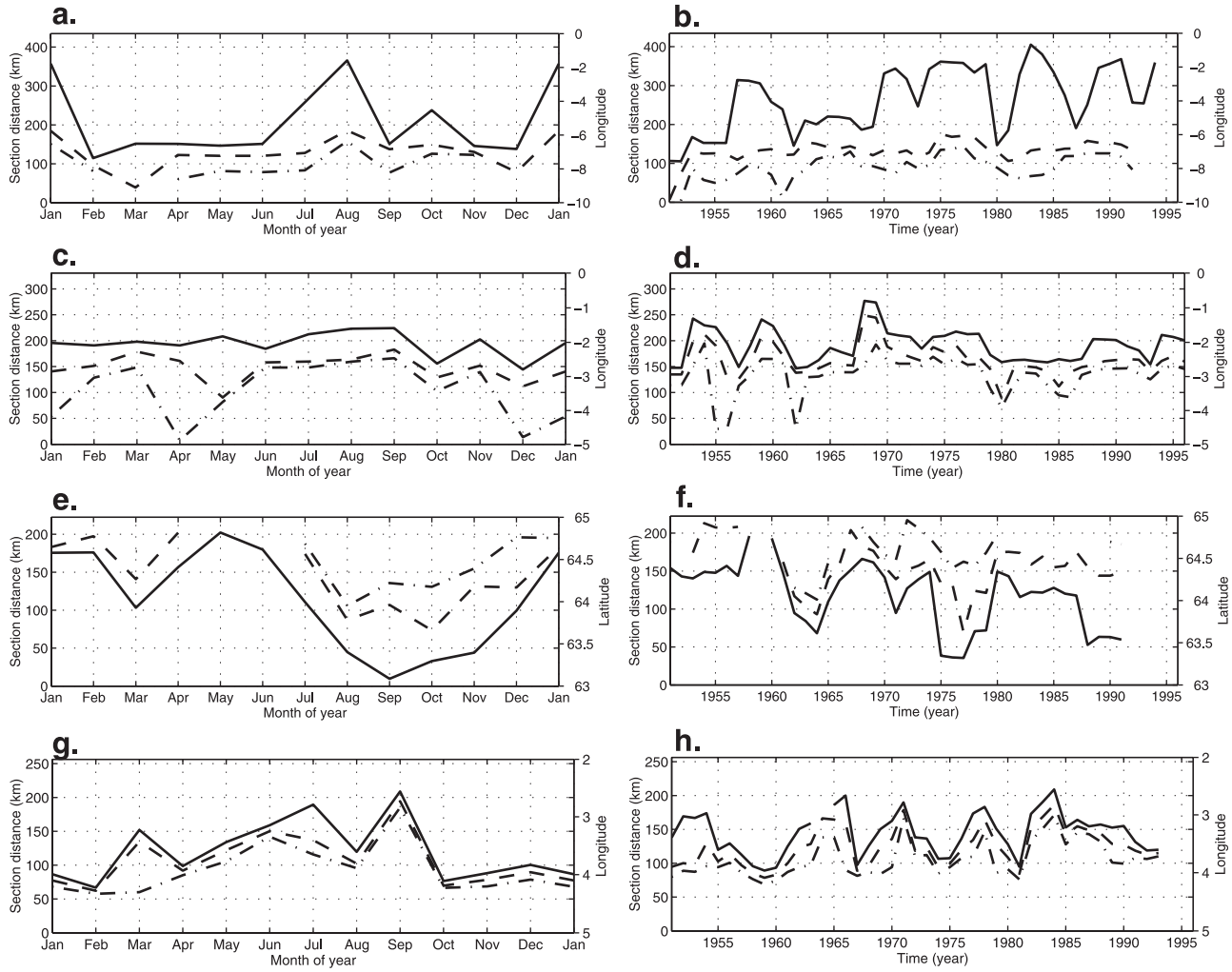

Figure 12. Seasonal and interannual variations in the sea surface positions of the 34.8, 34.9, and 35.0 psu isohalines from the four sections defined in Figure 10. Positions are found by averaging over the particular month for all years (left panels) or over 3 year periods centered at the particular year (right panels).

the SSS within the Nordic Seas, and results are therefore not presented here.

5. Surface Signatures of Subsurface Processes

5.1. Correlations Between the Surface and the Deeper Water

[42] As the focus of this study has been the variability in the SSS, it is of great interest to know to what extent signals in the SSS are expressions of subsurface salinity variations. If there are significant correlations between the surface signatures and the anomalies in the water body below, surface measurements can be used to detect anomalies propagating with the mean flow. A similar discussion has been carried out for temperature measurements in the Nordic Seas [*Furevik*, 2000, 2001]. Here satellite-derived SST anomalies were compared to anomalies found in several standard hydrography sections,

Table 1. Characteristics of Salinity Frontal Features in The Nordic Seas

Characteristic salinity feature	Mean frontal gradient (psu/km)	High-frequency temporal variability (standard) (psu)	Seasonal variability/ displacements (psu/km)	Interannual displacements (km)
Polar front (east–west)	0.5/500 (south) 0.5/150 (north)	0.04/0.01 0.04/0.01	0.01/150 0.01/50	300 180
Iceland Gap front (south–north)	0.5/250	0.03/0.01	0.1/60	150
Norwegian shelf break front (east–west)	0.5/100	0.06/0.02	0.1/40	60

The fronts are defined in Figures 10 and 11. The high-frequency variability is shown for September/March based on simulated SSS for the Polar and Iceland Gap fronts and on observations at OWSM for the Norwegian shelf break front. For the seasonal and interannual variability, typical displacements in the 35 psu isohaline (typical definition of the extension of the Atlantic Water) over a season or over 3 years are shown.

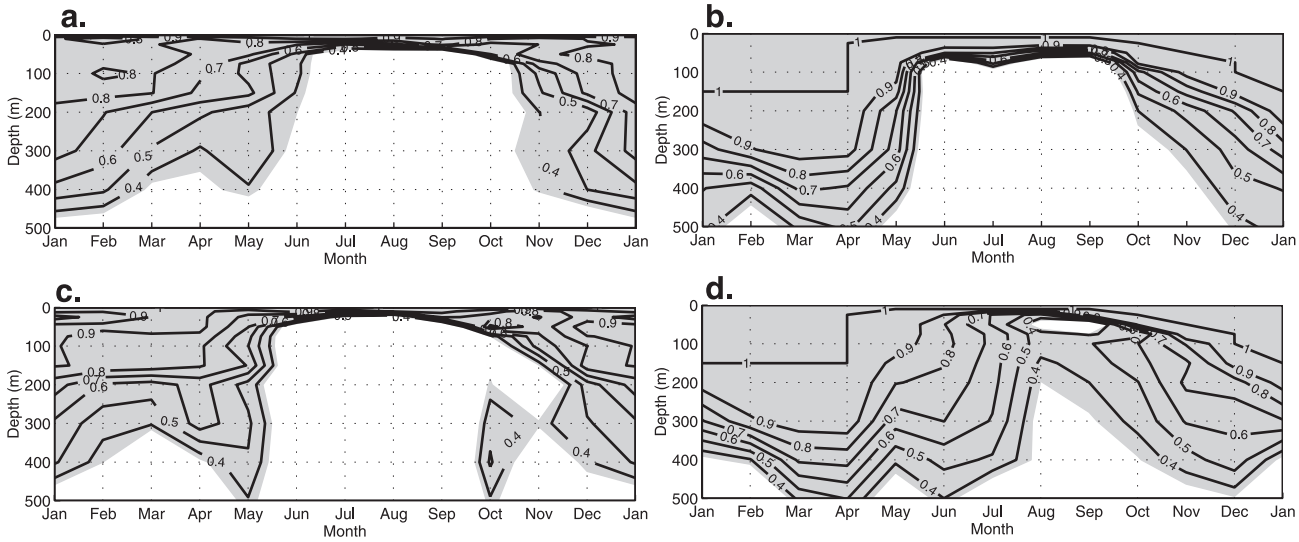

Figure 13. Correlation between monthly mean sea surface and subsurface anomalies of salinity (upper) and temperature (lower) at OWSM. The left (right) panels display observations (model simulations). The plots of salinity (temperature) have been made by correlating time series of SSS (SST) month by month with the corresponding time series at all other depths. Gray shading indicates the 99% significance levels.

showing a reasonable good concordance during the winter months.

[43] From monthly mean OWSM data, we have made subsets for each of the 12 months in a year, and calculated the correlations between the surface anomalies in salinity and temperature, and the corresponding anomalies in the waters below (Figure 13). For salinity (upper left panel), there is generally a high correlation between the surface and the subsurface waters for the months November to May. Here a correlation of 0.5 is found down to 200 m, and of 0.4 down to 400 m. This correlation is significant at the 99 percent level. Maximum correlation is found in January, with a near 0.6 correlation between surface and 400 m. For the months June to October, the surface salinity is uncorrelated with salinity in the waters below a few tens of meters. The physical reason for the difference is caused by the annual variation in the surface forcing and the corresponding density stratification, allowing enhanced vertical mixing during the winter months and the creation of an effective barrier between the surface and the subsurface waters in summer.

[44] The correlation plot for temperature shows the same pattern as the salinity plot (Figure 13c). During summer, correlations between surface and subsurface waters are lower, and during autumn it takes longer time before the correlations have been restored to the winter values.

[45] In comparison, the model simulated winter and summer ML is too deep, resulting in an overestimation of the correlation between the surface water and the waters below for both salinity and temperature. However, for salinity the results shown are not too far from the observed, with high vertical correlation during the months November to April. There is a larger discrepancy between the modeled and the observed temperature correlations, probably related to the problems with simulating the correct water masses and thus the stratification in the OWSM area, as discussed in section 3.

[46] A very dense data coverage is needed in order to calculate the spatial distribution in the correlation between surface signatures and deep ocean anomalies. Simple statistical analysis shows that the observational data are insufficient, so the correlations maps are only calculated based on the model fields (Figure 14). As for the OWSM position, there is a clear difference in the vertical correlation between the winter and the summer months for the entire region. During winter the correlation between the surface salinity and the 200 m depth salinity is exceeding 0.95 for most of the Norwegian Sea. In the central parts, the corresponding numbers for 400 m depth are typically ranging from 0.4 to 0.8, with maximum exceeding 0.95 in the central parts of the Norwegian Sea and to the south of Iceland, where the ML is deep. In the same areas the high-frequency variability shows a minimum (Figure 8). In areas where fresh Coastal or Polar Waters are on top of more saline waters, stratification is prominent and the correlation between surface and subsurface waters is lower.

[47] In summer, here represented by September, the correlations between the surface and 200 m depth is below 0.4 in the eastern part of the Nordic Seas, while local maxima of 0.6–0.7 are found in the central part of the basin. Furthermore, between surface and 400 m the correlation exceeds 0.5 only in the marginal ice zone, in the central Norwegian Sea, and south of the Faroe–Shetland inflowing area.

5.2. Implications for Deep Water Formation

[48] The Greenland Sea is one of the main formation sites for the dense deep and bottom waters of the World Oceans. In the central parts of the Nordic Seas, Atlantic Water is modified through intense surface cooling and mixing with waters of Arctic origin. When the modified water mass becomes sufficiently dense, it sinks and gradually spreads across the Nordic Seas. Eventually it spills over the ridges between Iceland and Scotland [*Hansen et al.*, 2001], from where it continues to sink, and by entrainment, forms the bottom water of the North Atlantic Ocean [*Dickson and Brown*, 1994].

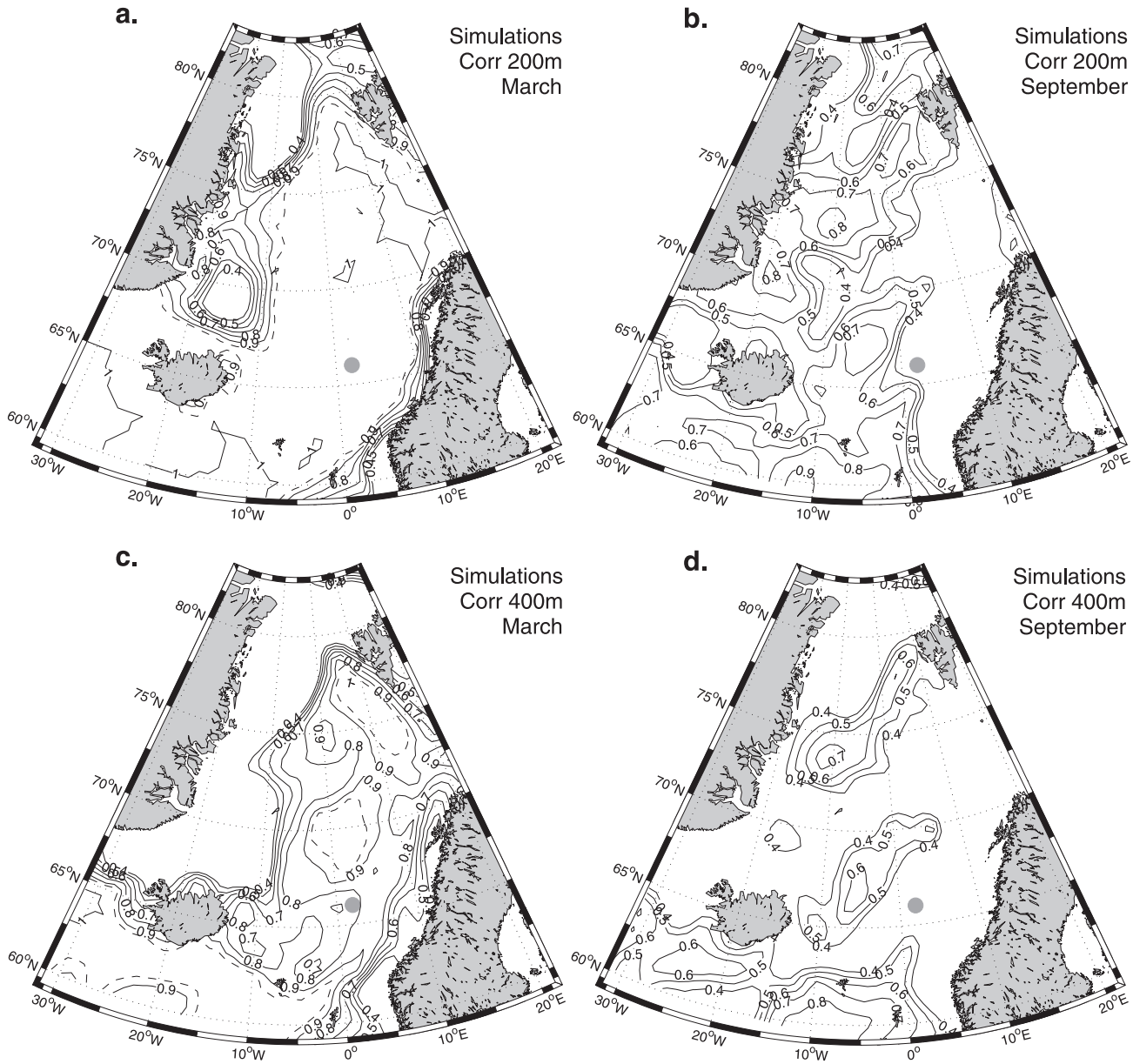

Figure 14. Correlation between SSS and salinities at 200 m (upper panels) and 400 m (lower panels) for March (left row) and September (right row). The position of OWSM is marked with a gray dot.

[49] During the last couple of decades, the convective activity in the Greenland Sea has been reduced and even shut down for periods [*Dickson et al.*, 1996], resulting in a freshening of the intermediate waters of the Nordic Seas [*Blindheim et al.*, 2000], a warming of the deep waters [*Østerhus and Gammelsrød*, 1999], and possibly reduced flow of dense water over the Iceland–Scotland ridges [*Hansen et al.*, 2001].

[50] The effect of even modest variations in salinity can be illuminated by examining the upper ocean density anomalies, and the fraction described by the salinity and temperature anomalies separately. The annual mean density distribution of the Nordic Seas is depicted in Figures 15a and 15b. It follows that the densest waters are found in the central Greenland and Iceland Seas, where the potential density averaged over 50–200 m exceeds 28.00 and 27.95, respectively. These are the main open ocean convection sites in the region [*Dickson and Brown*, 1994]. Note also that in the Greenland Sea, the maximum density at 50–200 m is located west of the maximum surface density.

[51] The vertical stratification is extremely weak, particularly in the Greenland Basin, and even small perturbations in the surface water density can have large impacts on the convection depths and deep water formation activities. There is a clear seasonal signal in the density in the central parts of the Greenland Sea (Figure 15c), with highest densities found in May and lowest in December. The seasonal signal in the density resembles the seasonal signal of temperature with a two months time lag (temperature minimum prior to density maximum) due to the salinity effect.

[52] We also find interannual variability in the density (Figure 15d), with high densities in the late 1960s, and low

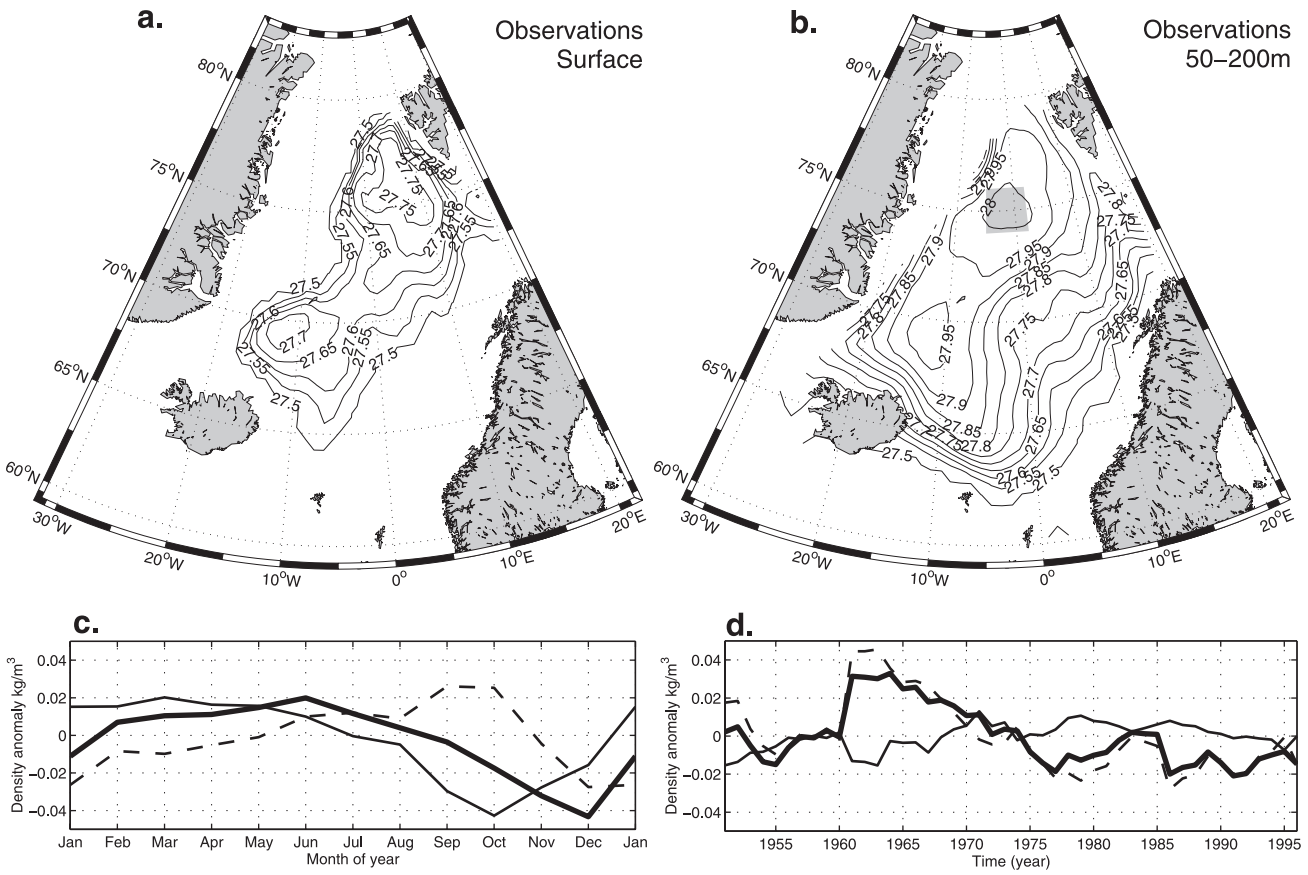

Figure 15. Annual mean potential density distribution (in σ_0) at 0 m (upper left panel) and averaged over 50–200 m (upper right panel). Lower panels show the seasonal and interannual deviation from the mean density at 50–200 m (1028.01 kg m^{-3}) in the area defined by the box $-5°W <$ to $< 2°E$ and $74°N <$ to $< 76°N$ (shaded rectangle in upper right panel). Together with the actual density anomalies (thick solid line), the contributions from the temperature and salinity anomalies are shown as the thin solid and dashed lines in the lower panels, respectively. The values are monthly climatology (lower left panel) or 3 year sliding means centered at the particular year (lower right panel).

densities in the latter part of the 1970s and onward. Separation of the density anomalies into the thermal and haline expansion terms shows that the major factor for determining the density at 50–200 m depth is salinity. There has been a week cooling trend of the water masses during the period 1950–1995. However, the impact of this cooling on density is far less than the effect of the freshening trend occurring during the same period. Since the 1960s, the combined effect of temperature and salinity has resulted in a gradually lighter upper water column, which is less favorable for convection.

6. Summary and Concluding Remarks

[53] For the first time a combination of the unique long term hydrographic data from OWSM [*Gammelsrød et al.*, 1992] and Russian data of the Norwegian and Greenland Seas [*Johannessen et al.*, 2000], together with numerical ocean model results based on MICOM [*Bleck et al.*, 1992], has been used to study the temporal and spatial variability of the SSS in the Nordic Seas. The following major findings have been revealed:

1. The day-to-day variability in the SSS varies with location and season and is largest in vicinity of frontal boundaries and in areas with the strongest stratification. At OWSM the lowest (0.03 psu) variability is in March and the highest (0.07 psu) in July due to the seasonal variations in atmospheric forcing and the corresponding thickness of the oceanic ML.

2. The SSS in the waters of Atlantic origin shows a maximum during winter and a minimum during summer as a result of increased surface heat flux and wind driven upper layer mixing in winter in contrast to freshening and surface warming of the upper layer coupled with reduced wind mixing during summer.

3. Investigation of the interannual variability in the last 50 years shows a marked freshening of the Atlantic Water in the Norwegian and Greenland Seas, less favorable for convective overturning. Moreover, the water masses along the western boundary of the inflowing Atlantic Water (i.e., southern Polar front), here defined by the 35 psu isohaline, undergo near zonal migrations on seasonal to interannual timescales of up to 300 km. In contrast the 35 psu isohaline along the sharper fronts defining the northern part of the Polar front, and the continental shelf break front off Norway are only capable to migrate typically between 60 and 80 km.

4. During winter the SSS shows strong correlation (0.5) with the subsurface salinity values down to more than

200 m as a result of vertical mixing, whereas the SSS is uncorrelated with the subsurface salinity below a few tens of meters due to surface freshening and limited vertical mixing during summer.

5. In the central Greenland Sea the seasonal cycle in upper ocean density is governed by the temperature, while interannual variability is governed by the salinity variations. Since the 1960s there has been a rapid decrease in the salinity, with respect to the density more than compensating for the small warming during the same period. This suggests a reduction in the intensity of the deep water formation, in concordance of what has been reported.

[54] Examination of these results in the context of deep water formation and climate variability have clearly identified the important role of the upper ocean salinity for the thermohaline circulation. It is expected that finer model resolution and/or model subgrid scale parameterizations will yield better simulation of the evolution of the salinity fields in the Nordic Seas. However, access to regular SSS fields from in situ and satellite observing systems to constrain the model is perhaps more demanding in order to advance the capability to simulate and examine the major modes of the natural fluctuations of the ocean system and its importance for climate.

[55] **Acknowledgments.** Thanks to Svein Østerhus at the Bjerknes Center and the Geophysical Institute, University of Bergen, for kindly providing the hydrographic data from the OWSM and to the anonymous reviewers whose critical remarks improved the quality of the paper. This work has been supported by the Norwegian Research Council through the RegClim and NOClim projects, the Bjerknes Collaboration for Climate Research (MB), and the Programme of Supercomputing and by the ESA study contract 14273/00/NL/DC.

References

Arakawa, A., and V. R. Lamb, Computational design of the basic dynamical processes of the UCLA General Circulation Model, in *Methods in Computational Physics*, vol. 13, pp. 173–265, Academic, San Diego, Calif., 1977.

Bentsen, M., and H. Drange, Parameterizing surface fluxes in ocean models using the NCEP/NCAR reanalysis data, in *Regional Climate Development Under Global Warming, Gen. Tech. Rep.*, *4*, pp. 149–157, Norw. Inst. for Air Res., Kjeller, Norway, 2000.

Bentsen, M., G. Evensen, H. Drange, and A. D. Jenkins, Coordinate transformation on a sphere using conformal mapping, *Mon. Weather Rev.*, *127*, 2733–2740, 1999.

Bleck, R., C. Rooth, D. Hu, and L. T. Smith, Salinity-driven thermocline transients in a wind- and thermohaline-forced isopycnic coordinate model of the North Atlantic, *J. Phys. Oceanogr.*, *22*, 1486–1505, 1992.

Blindheim, J., V. Borovkov, B. Hansen, S. A. Malmberg, W. R. Turrell, and S. Østerhus, Upper layer cooling and freshening in the Norwegian Seas in relation to atmospheric forcing, *Deep Sea Res.*, *47*, 655–680, 2000.

Dickson, R. R., and J. Brown, The production of North Atlantic Deep Water: Sources, rates, and pathways, *J. Geophys. Res.*, *99*, 12,319–12,341, 1994.

Dickson, R. R., J. Meincke, S.-A. Malmberg, and A. J. Lee, The "Great Salinity Anomaly" in the northern North Atlantic 1968–1982, *Prog. Oceanogr.*, *20*, 103–151, 1988.

Dickson, R. R., J. Lazier, J. Meincke, P. Rhines, and J. Swift, Long-term coordinated changes in the convective activity of the North Atlantic, *Prog. Oceanogr.*, *38*, 241–295, 1996.

Drange, H. and K. Simonsen, *Formulation of Air–Sea Fluxes in the ESOP2 Version of MICOM, Tech. Rep. 125*, 23 pp., Nansen Environ. and Remote Sens. Cent., Solheimsviken, Norway, 1996.

Fairall, C. W., E. F. Bradley, D. P. Rogers, J. B. Edson, and G. S. Young, Bulk parameterization of air–sea fluxes for Tropical Ocean–Global Atmosphere Coupled-Ocean Atmosphere Response Experiment, *J. Geophys. Res.*, *101*, 3747–3764, 1996.

Fichefet, T., and P. Gaspar, A model study of upper ocean–sea ice interaction, *J. Phys. Oceanogr.*, *18*, 181–195, 1988.

Friedrich, H., and S. Levitus, An approximation to the equation of state for seawater, suitable for numerical ocean models, *J. Phys. Oceanogr.*, *2*, 514–517, 1972.

Furevik, T., On anomalous sea surface temperatures in the Nordic Seas, *J. Clim.*, *13*(5), 1044–1053, 2000.

Furevik, T., Annual and interannual variability of Atlantic Water temperatures in the Norwegian and Barents Seas: 1980–1996, *Deep Sea Res.*, *48*, 383–404, 2001.

Gammelsrød, T., S. Østerhus, and Ø. Godøy, Decadal variations of ocean climate in the Norwegian Sea observed at Ocean Station "Mike" (66°N 2°E), *ICES Mar. Sci. Symp.*, *95*, 68–75, 1992.

Gargett, A., Vertical eddy diffusivity in the ocean interior, *J. Mar. Res.*, *42*(2), 359–393, 1984.

Gaspar, P., Modeling the seasonal cycle of the upper ocean, *J. Phys. Oceanogr.*, *18*, 161–180, 1988.

Hansen, B., and S. Østerhus, North Atlantic–Norwegian sea exchanges, *Prog. Oceanogr.*, *45*, 109–208, 2000.

Hansen, B., W. R. Turrell, and S. Østerhus, Decrease of the overflow from the Nordic Seas into the Atlantic in the Faroe Bank Channel since 1950, *Nature*, *411*, 927–930, 2001.

Harder, M., *Dynamik, Rauhigkeit und Alter des Meereises in der Arktis*, PhD thesis, Alfred-Wegener-Inst. für Polar- und Meeresforsch., Bremerhaven, Germany, 1996.

Helland-Hansen, B., and F. Nansen, The Norwegian Sea: Its physical oceanography based upon the Norwegian researches 1900–1904, *Rep. Norw. Fish. Mar. Invest.*, *2*(1–2), 390, 1909.

Hibler, W., III, A dynamic thermodynamic sea ice model, *J. Phys. Oceanogr.*, *12*, 815–844, 1979.

Hurdle, B. G., (Ed.), *The Nordic Seas*, 777 pp., Springer-Verlag, New York, 1986.

Hurrell, J., Decadal trends in the North Atlantic Oscillation: Regional temperatures and precipitation, *Science*, *269*, 676–679, 1995.

Johannessen, O. M., Brief overview of the physical oceanography, in *The Nordic Seas*, edited by B. Hurdle, pp. 103–124, Springer-Verlag, New York, 1986.

Johannessen, O. M., et al., Detection and modelling of greenhouse warming in the Arctic and sub-Arctic. Oceanographic data analysis: Greenland Sea, *Technical Report on Task 3, INTAS 97-1277*, Nansen Environ. and Remote Sens. Cent./Arctic and Antarct. Res. Inst., Solheimsviken, Norway, 2000.

Kalnay, E., et al., The NCEP/NCAR 40-year reanalysis project, *Bull. Am. Meteorol. Soc.*, *77*(3), 437–471, 1996.

Levitus, S. and T. P. Boyer, *World Ocean Atlas 1994, Volume 4, Temperature*, NOAA Atlas NESDIS 4, Washington, D. C., 1994.

Levitus, S., R. Burgett, and T. P. Boyer, *World Ocean Atlas 1994, Volume 3, Salinity*, NOAA Atlas NESDIS 3, Washington, D. C., 1994.

McDougall, T. J., and W. K. Dewar, Vertical mixing and cabbeling in layered models, *J. Phys. Oceanogr.*, *28*, 1458–1480, 1998.

Orvik, K. A., Ø. Skagseth, and M. Mork, Atlantic inflow to the Nordic Seas: Current structure and volume fluxes from moored current meters, VM-ADCP and SeaSoar-CTD observations, 1995–1999, *Deep Sea Res.*, *48*, 937–957, 2001.

Østerhus, S., and T. Gammelsrød, The abyss of the Nordic Seas is warming, *J. Clim.*, *12*(11), 3297–3304, 1999.

Parkinson, C. L., and W. M. Washington, A large-scale numerical model of sea ice, *J. Geophys. Res.*, *84*, 311–337, 1979.

Semtner, A. J., A model for the thermodynamics growth of sea ice in numerical investigations of climate, *J. Phys. Oceanogr.*, *6*, 379–389, 1976.

Smolarkiewicz, P. K., A fully multidimensional positive definite advection transport algorithm with small implicit diffusion, *J. Comput. Phys.*, *54*, 325–362, 1984.

Smolarkiewicz, P. K., and T. L. Clark, The multidimensional positive definite advection transport algorithm: Further development and applications, *J. Comput. Phys.*, *67*, 396–438, 1986.

Zalesak, S., Fully multidimensional flux-corrected transport algorithms for fluids, *J. Comput. Phys.*, *31*, 335–362, 1979.

M. Bentsen, H. Drange, T. Furevik, and J. A. Johannessen, Nansen Environmental and Remote Sensing Center, Bergen, Norway.

A. Korablev, Arctic and Antarctic Research Institute, St. Petersburg, Russia.